Chaos, Solitons and Fractals 103 (2017) 307–324

Contents lists available at ScienceDirect

Chaos, Solitons and Fractals

Nonlinear Science, and Nonequilibrium and Complex Phenomena

journal homepage: www.elsevier.com/locate/chaos

Frontiers

Using 0–1 test to diagnose chaos on shape memory alloy dynamical systems

Marcelo A. Savi[a,*], Francisco Heitor I. Pereira-Pinto[a], Flavio M. Viola[b], Aline Souza de Paula[c], Davide Bernardini[d], Grzegorz Litak[e,f], Giuseppe Rega[d]

[a] Center for Nonlinear Mechanics, COPPE – Department of Mechanical Engineering, Universidade Federal do Rio de Janeiro, P.O. Box 68.503, 21.941.972, Rio de Janeiro, RJ, Brazil
[b] Department of Mechanical Engineering, CEFET/RJ, 20.271.110, Rio de Janeiro, RJ, Brazil
[c] Department of Mechanical Engineering, Universidade de Brasília, 70.910.000, Brasília, DF, Brazil
[d] Università di Roma - La Sapienza, Department of Structural and Geotechnical Engineering Via Antonio Gramsci 53, 00197, Rome, Italy
[e] Lublin University of Technology, Faculty of Mechanical Engineering Nadbystrzycka 36, 20-618, Lublin, Poland
[f] AGH University of Science and Technology, Department of Process Control Mickiewicza 30, PL-30-059, Cracow, Poland

ARTICLE INFO

Article history:
Received 6 February 2017
Revised 13 June 2017
Accepted 17 June 2017

Keywords:
Shape memory alloys
0–1 test
Lyapunov exponents
Chaos
Chaos diagnose
Nonlinear dynamics

ABSTRACT

Shape Memory Alloy (SMA) dynamical systems may exhibit a rich response that can include periodic, quasi-periodic, chaotic and hyperchaotic behaviors. In this regard, diagnostic tools are important in order to identify the different types of behaviors. This paper aims to analyze systems with SMA elements through a nonlinear dynamics perspective with a specific focus on the use of 0–1 test to quantify the chaoticity of the dynamical response of SMA oscillators. The investigation includes different constitutive models for the restitution force on both single- and two-degree of freedom oscillators. Results of the 0–1 test are compared with Lyapunov exponents calculated with different algorithms. The analyses show that the 0–1 test can be considered a reliable and computationally efficient alternative as a diagnostic tool of chaotic responses.

1. Introduction

Shape Memory Alloys (SMAs) are being used in several applications due to their remarkable thermomechanical behavior. Applied dynamics usually exploits SMA capacity to dissipate energy and to change properties due to solid phase transformations. Dynamical responses of SMA systems are very rich due to their strong nonlinearities. Because of that, the use of SMAs in dynamical applications requires a deep understanding of the system response [29].

Nonlinear dynamics investigations of SMA systems started in the 1990s [12,32] and since then, literature has several investigations treating their complex responses that include chaotic behavior. In general, numerical simulations are performed employing different constitutive models. The thermomechanical description of SMAs can be done in different ways and there exists several reviews of the state of the art about constitutive modeling, see e.g., Lagoudas [22] and Paiva et al. [27]. In this regard, the nonlinear dynamics analysis of SMA systems have some efforts that should be highlighted: Savi and Pacheco [31] employed the polynomial constitutive model treating both single and two-degree of freedom oscillators; Bernardini and Rega [4] employed the Bernardini–Pence's model; Savi et al. [30] employed the model with internal constraints [27]; Machado et al. [26] employed Boyd–Lagoudas' model. Besides, some experimental investigations attest the main conclusions related to numerical simulations: Enemark et al. [8,9]; Aguiar et al. [1]; Sitnikova et al. [33]; Machado [25].

The use of SMA to vibration reduction may be strongly influenced by the eventual presence of chaotic motions as they often occur in conjunction with strong jumps of response amplitude. Such jumps as well as the unpredictability of the response may drastically reduce, if not completely eliminate, the effectiveness of such devices. For this reason, reliable tools for chaos detection may be very important also in the design of SMA-based devices

Deterministic chaos is a possible response of SMA systems and a proper diagnose is one of the essential issues related to the system investigation. Lyapunov exponents constitute a well-established diagnostic tool for chaotic dynamical systems, and several algorithms can be employed to evaluate the Lyapunov spectrum. Lyapunov exponent calculation can be performed either from equations of motion or from time series. Concerning time series analysis, it is important to evaluate the robustness of each tech-

* Corresponding author.
E-mail addresses: savi@mecanica.ufrj.br (M.A. Savi), fmviola@gmail.com (F.M. Viola), alinedepaula@unb.br (A.S. de Paula), davide.bernardini@uniroma1.it (D. Bernardini), g.litak@pollub.pl (G. Litak), giuseppe.rega@uniroma1.it (G. Rega).

http://dx.doi.org/10.1016/j.chaos.2017.06.016
0960-0779/

nique due to noise contamination. In this regard, the algorithm due to Kantz [20] is a classical approach to estimate maximum Lyapunov exponent presenting low noise sensitivity. The algorithm due to Wolf et al. [36] is a classical approach for systems governed by ordinary differential equations that can be linearized around a reference trajectory. The hysteretic behavior of SMAs introduces difficulties for the application of this method. Machado et al. [26] proposed an approach to employ the algorithm due to Wolf et al. [36] on hysteretic systems.

The 0–1 test has been used as an interesting alternative to diagnose chaos in dynamical systems, being of special interest for systems where the classical approaches are difficult to be applied. In brief, this is a statistical approach based on the asymptotic properties of a Brownian motion chain. Gottwald and Melbourne [14,15] presented this procedure to distinguish chaotic from regular behavior in deterministic systems. The test provides, as a result, a number that lies between 0 and 1. If the dynamical behavior of the tested system is chaotic, the result is close to 1, or close to 0 if the system exhibits non-chaotic or regular behavior. Gottwald and Melbourne [18] and Bernardini and Litak [2] presented general overviews of the theoretical background and the use of 0–1 test for chaos diagnose.

The 0–1 test can be applied directly to time series and therefore is independent on the nature of the underlying dynamical system [16,17]. Litak et al. [23] and Bernardini et al. [7] applied the 0–1 test to SMA systems considering time series obtained from numerical simulations of equations of motion. Different applications of the test can be found in several research efforts. Falconer et al. [10] applied the test to an experimental time series from a bipolar motor. Webel [35] employed this method for testing chaos in the return time series from the German stock market. Other interesting applications of the 0–1 test can be found on Krese and Govekar [21] and Yuan et al. [38].

This paper discusses the application of the 0–1 test to SMA systems and investigates its effectiveness in the detection of chaotic responses establishing a comparison with the Lyapunov exponents. Moreover, since SMA exhibits a complex thermomechanical response and several constitutive models have been proposed in the literature, the analysis includes the performances of the diagnostic tools on three different SMA models: polynomial model [11,31]; model with internal constraints [27,30], Bernardini–Pence's model [3–6]. Moreover, single- and two-degree of freedom systems are analyzed allowing one to obtain a proper comprehension of the general behavior of SMA systems, investigating different system dimensions. It is beyond the scope of this contribution the comparison of the SMA models. Time series are generated from the equations of motion and results obtained with the 0–1 test are compared with Lyapunov exponents. Basically, the algorithms due to Wolf et al. [36] and Kantz [20] are employed for the estimation of the exponents. The main goal is to evaluate the 0–1 test capacity to diagnose different kinds of response.

Two different archetypal systems are evaluated considering distinct dimensions: single-degree of freedom system, 1-dof (Fig. 1a); two-degree of freedom system, 2-dof (Fig. 1b). Essentially, the single-degree of freedom system is an oscillator with a mass, m, with a displacement u, connected to the support by an SMA element and a linear viscous damper with coefficient c, and subjected to a harmonic excitation $F = \bar{F}\sin(\Omega t)$. The two-degree of freedom system consists of two coupled oscillators with masses, m_i $(i = 1,2)$, connected by SMA elements and linear dampers with coefficient c_i $(i = 1,2,3)$. Each mass has displacement u_i $(i = 1,2)$ being harmonically excited by an external force $F_i = \bar{F}_i\sin(\Omega_i t)$ $(i = 1,2)$.

After this introduction, the paper is organized as follows. Initially, a brief description of the diagnostic tools is presented, emphasizing Lyapunov exponents and 0–1 test. Numerical simulations are then carried out for different models, starting with single-degree of freedom systems. Polynomial, internal constraints and Bernardini–Pence models are treated. Afterwards, a two-degree of freedom system described with polynomial model is investigated. Concluding remarks are then discussed.

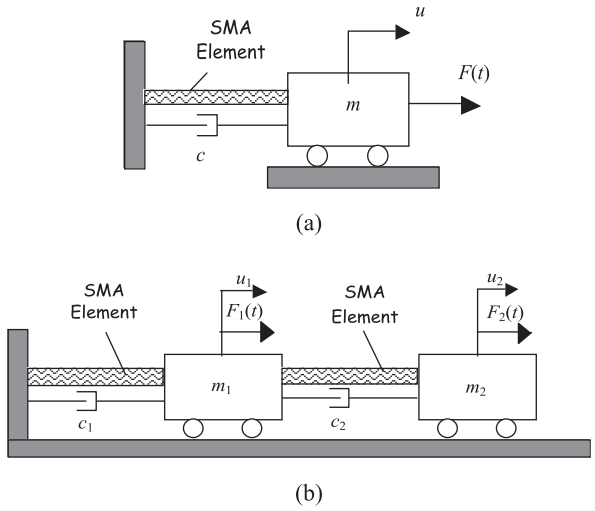

Fig. 1. SMA dynamical systems. (a) single and (b) two degree-of-freedom mass systems.

2. Diagnostic tools

Nonlinear dynamics of SMA systems is very rich, being associated with complex responses. In this regard, periodic, quasiperiodic, chaotic and hyperchaotic solutions can arise and it is important to employ suitable diagnostic tools that allow a proper identification of these behaviors. Usually, the estimation of some system invariant is adopted and the most widely used is the Lyapunov exponents.

The classical algorithm due to Wolf et al. [36] can be considered a well-established procedure when equations of motion are available. Nevertheless, its use needs the determination of a system linearization that is not an easy task for hysteretic systems, where complex, generally non-smooth, constitutive equations are usually employed. In this regard, there is the alternative of a time series analysis where Kantz [20] algorithm is an interesting approach. The 0–1 test proposed by Gottwald and Melbourne [14] is another interesting alternative for time series analysis.

2.1. Lyapunov exponents

The set of Lyapunov exponents is a system invariant that estimates its sensitivity to initial conditions by evaluating local divergence of nearby orbits. It represents one of the most accepted diagnostic tool for chaos. In brief, the divergence of nearby orbits can be analyzed monitoring the distance between a reference orbit and its neighboring orbits while the system evolves through time. If the measured distance increases, there is a local divergence that characterizes chaos. Chaotic response is, therefore, associated with at least one positive value, representing a divergent direction.

Usually, the reference orbit is evaluated from the equations of motion and the nearby orbit evolution is monitored by an extension of the equations of motion. Wolf et al. [36] presented a procedure where this extension is evaluated from a linearized version of the dynamical system. Besides, new initial conditions are adopted for each time step, avoiding an explosive behavior.

The algorithm due to Kantz [20] employs a similar idea where the distances between two orbits increase with a rate given by the

largest Lyapunov exponent. This algorithm establishes that the orbits divergence rate fluctuates, with the fluctuation given by the spectrum of effective Lyapunov exponents. This rate of divergence oscillates through time, as measured around the direction of instability. The determination of the largest Lyapunov exponent is related to the slope of the curve $S(\tau)$ that represents distances as a function of a relative time (τ) associated with local divergence. The slope determination is calculated between the initial value and the point at which the curve $S(\tau)$ has a horizontal trend; a linear fit using least square method can be applied for this aim. Kantz algorithm presents better results when applied to maps and therefore, Poincaré map time series is employed together with state space reconstruction.

The basic idea of the state space reconstruction is that a system observation time series contains information about unobserved state variables. Hence, the observation of a single state variable is enough to define the present state. Therefore, a scalar time series, $s(t)$, may be used to build a vector time series that is equivalent to the original dynamics from a topological point of view [34]. The state space reconstruction can be performed by different techniques. Delayed coordinates is an interesting alternative to capture the structure of orbits in state space using lagged variables, $s(t+\bar{\tau})$, where $\bar{\tau}$ is the time delay. Hence, it is possible to use a collection of time delays to create a vector in a D_e -dimensional space,

$$u(t) = \{s(t),\ s(t+\bar{\tau}),\ \ldots,\ s(t+[D_e-1]\bar{\tau})\} \tag{1}$$

Delay parameters, time delay and embedding dimension, need to be evaluated using proper procedures. Time delay is usually analyzed using the method of average mutual information [13]. The idea is to use the average mutual information to seek for delays related to minimum information between the two delayed vectors. The smaller values makes the two vectors more independent and therefore, more appropriate to represent state variables. Therefore, the choice is usually related to the first global minimum of the information-delay curve. False nearest neighbors can be employed to evaluate embedding dimension [28]. The idea is to seek for false neighbors by the increase of system dimension. The embedding dimension is found when false neighbors do not exist due to the dimension increase.

In this work, Wolf et al. algorithm is employed together with Kantz algorithm to evaluate Lyapunov exponents. It should be pointed out that the Wolf et al. algorithm furnishes the whole spectrum of exponents and needs the equations of motion. On the other hand, Kantz algorithm furnishes the maximum exponent, being calculated from time series obtained from equations of motion. Since system dimension is known, embedding dimension is considered to be the dimension of the equations of motion system. Tisean package is employed to estimate time delay and Lyapunov exponent due to Kantz [19]. Otherwise mentioned, default time delay is employed.

2.2. 0–1 test

The 0–1 test was originally proposed by Gottwald and Melbourne [14,15] to distinguish chaotic and regular dynamics. In brief, it is a statistical approach based on the asymptotic properties of a Brownian motion chain. The 0–1 test can be directly applied to time series and therefore does not require phase space reconstruction since it is based on the analysis of the features of a single coordinate of the dynamical system. Hence, it is independent on the nature of the underlying dynamical system evaluating the long-term system behavior that can be used as a diagnostic tool for chaos [18].

The test can be performed by analyzing any observable quantity $x_j (j = 1, \ldots, N)$ related to the system evolution. Typically, the time evolution of one of the state components suffices but other quantities could be used as well. Poincaré map time series of some state variable is employed in this work.

The basic idea of 0–1 test hinges on the definition of a dynamical system extension characterized by two additional variables, $p = p(n, c)$ and $q = q(n, c)$, which are driven by the system dynamics [2]. Specifically, Gottwald and Melbourne [16] proposed the following definition:

$$\begin{aligned} p(n) &= \sum_{j=1}^{n} x_j \cos(jc) \\ q(n) &= \sum_{j=1}^{n} x_j \sin(jc) \end{aligned} \tag{2}$$

where $n = 1, \ldots, N$ and $c \in [0, \pi]$ is a constant. Different values of c yields different p–q dynamics and for some values of c the latter can show resonance-like phenomenon that has to be considered as exceptional spurious outliers to be excluded from the analysis. In order to limit the occurrence of such resonances that can promote distortion of the results, the constant c is limited to the interval $[\pi/5, 4\pi/5]$ as suggested by Gottwald and Melbourne [16].

The variables p and q evolve in time as a consequence of the evolution of the observable x and therefore, they reflect information about the system dynamical response. The theory underlying the test ensures that if the system dynamics is regular, variables p and q exhibit a bounded evolution; on the other hand, if the underlying dynamics is chaotic these variables exhibits asymptotically unbounded growth with features reminiscent of Brownian motion [2,14,16]. Fig. 2 shows p–q space considering regular and irregular motions where it is clearly identified the different evolution of both situations.

The identification of chaos by means of 0–1 test requires to find a synthetic indicator of the unboundedness of the p–q dynamics. The mean-square displacement (MSD) can be employed for this aim,

$$M_c = \lim_{N\to\infty} \frac{1}{N} \sum_{j=1}^{N} \left[(p_c(j+n) - p_c(j))^2 + (q_c(j+n) - q_c(j))^2 \right] \tag{3}$$

where N is the signal total number of points and n is the size of time-lags over which the displacements are evaluated. In fact, the bracketed term in the sum represents the square of the displacement in the p–q-plane from the time j to the time $j+n$ so that M_c expresses the mean of all such squared displacements evaluated for all possible time lags over the whole trajectory.

The theory behind the 0–1 test assures that if the dynamics is regular, M_c is a bounded function of time. On the other hand, if the dynamics is chaotic, M_c scales linearly with time.

Alternatively, the test can be based on a modified least square displacement, $D_c = D_c(n)$, which exhibits the same asymptotic growth of M_c but with better convergence properties [16]:

$$D_c = M_c - \left(\lim_{N\to\infty} \frac{1}{N} \sum_{j=1}^{N} x_j \right)^2 \frac{1-\cos(nc)}{1-\cos(c)} \tag{4}$$

After the calculation of M_c or D_c, the sought indicators are provided by any measure K of their asymptotic growth rate. To this end, two different methods can be employed: regression and correlation methods. Therefore, 0–1 test can be implemented by using four possible chaos indicators combining M_c and D_c with regression and correlation methods, named K-metrics that are summarized in Table 1.

The regression method defines a straight line fitted to the logarithmic graph of the MSD against n, minimizing the square deviations. This estimation employs the least square method to mini-

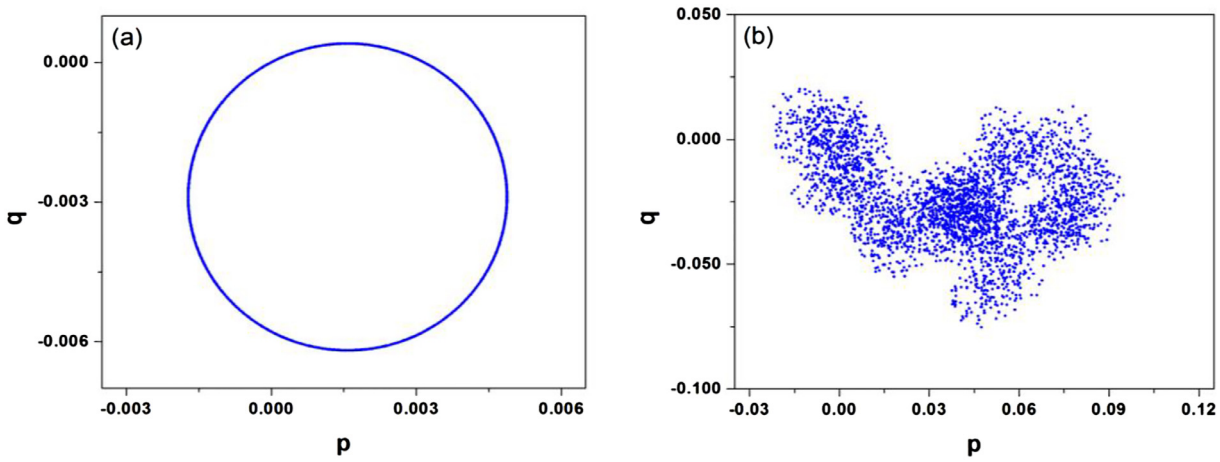

Fig. 2. General plot of p–q dynamics. Regular (a) and irregular (b) responses.

Table 1
Different approaches for K estimation.

K-metrics	Name	Employed method	MSD metric
K_r	M-Regression	Regression	$M_c\ (n)$
K_c	M-Correlation	Correlation	$M_c\ (n)$
K_r^*	D-Regression	Regression	$D_c\ (n)$
K_c^*	D-Correlation	Correlation	$D_c\ (n)$

Table 2
Parameters of the single-dof polynomial model.

ϖ	ξ	ϕ	γ
1.0	0.1	1.3×103	4.7×105

mize the residuals of the linear model. Therefore, the two possibilities are:

$$K_r = \lim_{n\to\infty} \frac{\log[M_c]}{\log[n]} \tag{5}$$

$$K_r^* = \lim_{n\to\infty} \frac{\log[D_c]}{\log[n]} \tag{6}$$

The second approach considers a correlation method, defining the chaos indicator K as the correlation between the MSD and linear growth defined as ratio between the covariance, cov(x,y), and the product of the standard deviations or variance, var(x),

$$K_c = \mathrm{corr}(\zeta, M) = \frac{\mathrm{cov}(\zeta, M)}{\sqrt{\mathrm{var}(\zeta)\mathrm{var}(M)}} \tag{7}$$

$$K_c^* = \mathrm{corr}(\zeta, D) = \frac{\mathrm{cov}(\zeta, D)}{\sqrt{\mathrm{var}(\zeta)\mathrm{var}(D)}} \tag{8}$$

where $\zeta = 1, 2, \ldots, n$; $M = (M_c(1), M_c(2), \ldots, M_c(n))$ and $D = (D_c(1), D_c(2), \ldots, D_c(n))$. Although correlation measurements belong to $[-1, +1]$, Gottwald and Melbourne [17] presented a proof that this type of correlation is actually in [0, 1].

The indicators K provide information about the asymptotic behavior of the p–q dynamics that is driven by the system dynamics through the definition, Eq. (2). However, as anticipated before, the relation between p–q dynamics and the system dynamics depends on the parameter c that enters definition. Therefore, different values of c produce different values for K and eventual resonance-like phenomenon associated with exceptional values of c can produce spurious values of K. In order to neutralize this effect, Gottwald and Melbourne [16] suggested to repeat the evaluation of K several times with different values of c (experience then shows that $N_c = 100$ is sufficient to get reliable results) and take, as final indicator for chaos, the median of all outcomes of K.

Gottwald and Melbourne [16] have shown that the application of the 0–1 test for continuous system needs to be associated to a proper sampling, with sampling rate smaller than the Nyquist rate. In this regard, these authors suggested the use of the mutual information to determine a satisfactory sampling rate [37].

3. SMA polynomial model

The polynomial model proposed by Falk [11] is based on Devonshire's theory and considers a polynomial free energy density as a function of strain, ε, and temperature, T, and does not consider any other internal variable. The form of the free energy is chosen in such a way that the minima and maxima points respectively represent stability and instability of each macroscopic phase of the SMA. The polynomial is proposed in order to represent three macroscopic phases: austenite (A) and two variants of martensite ($M+$, $M-$). Hence, the free energy is chosen such that for high temperatures it has only one minimum at vanishing strain, representing the equilibrium of the austenitic phase. At low temperatures, martensite is stable, and the free energy must have two minima at non-vanishing strains. At intermediate temperatures, the free energy must have equilibrium points corresponding to both phases. Therefore, the stress-strain-temperature relation is a fifth-order polynomial that represents the general behavior of SMAs. Under these assumptions, force-displacement relation is a nonlinear elastic curve that represents the thermomechanical equilibrium. An equivalent linear viscous damper is employed to represent hysteretic dissipation aspects. Despite its simplicity, this model furnishes a good qualitative description of SMA dynamical response.

Based on that, assuming dimensionless variable y_0, related to displacement, and y_1, associated with velocity, the dimensionless equations of motion is given by [31],

$$\begin{aligned} \dot{y}_0 &= y_1 \\ \dot{y}_1 &= \delta \sin(\varpi t) - \xi y_1 - (\theta - 1) y_0 + \phi y_0^3 - \gamma y_0^5 \end{aligned} \tag{9}$$

where dot represents time derivative, δ and ϖ are excitation parameters; ξ is related to dissipation; θ represents the temperature; ϕ and γ are SMA constitutive parameters. Table 2 presents the parameters employed for all simulations [24].

Numerical simulations are performed by employing a fourth-order Runge-Kutta scheme with time steps smaller than

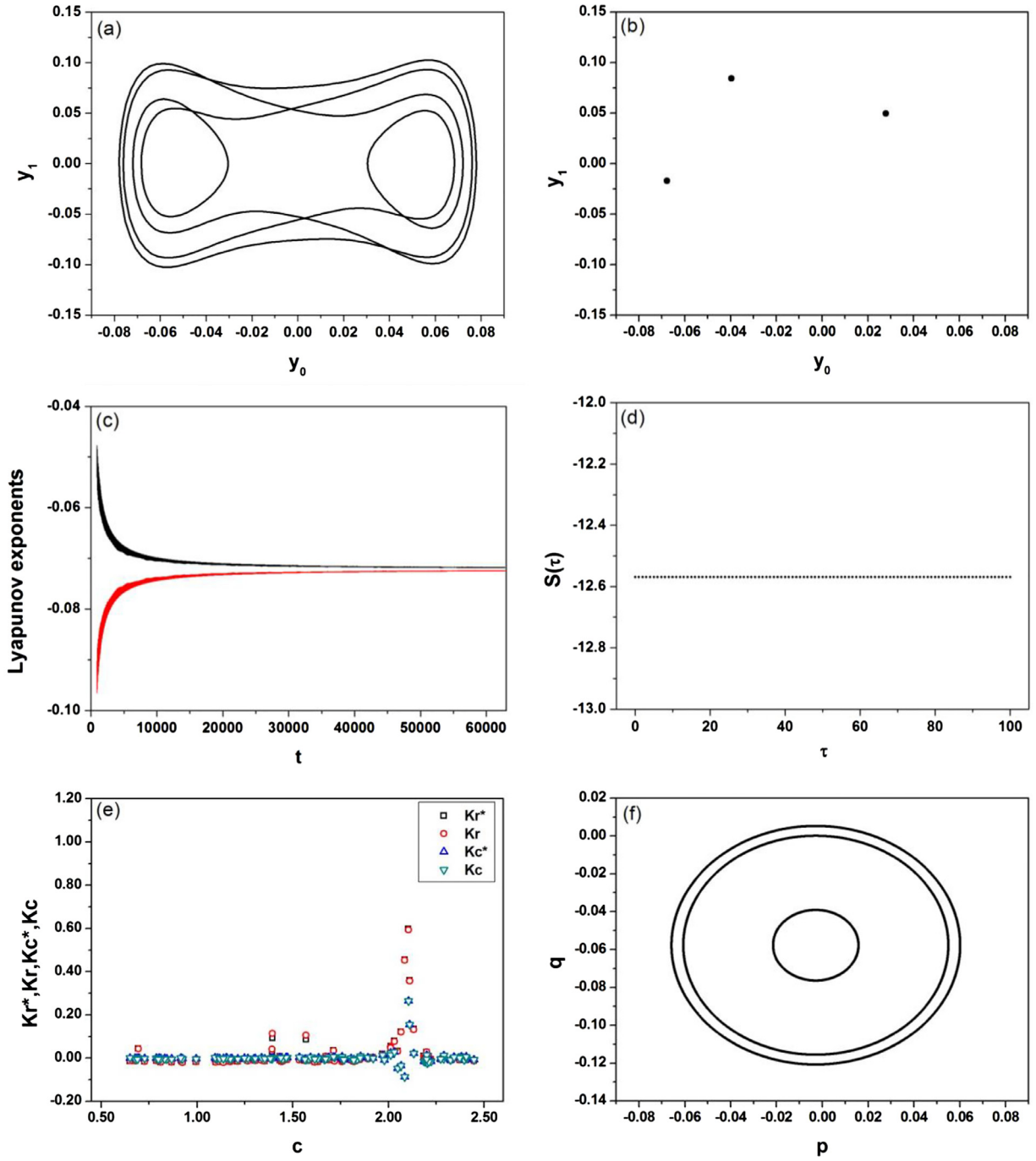

Fig. 3. Polynomial model - periodic motion ($\delta = 0.038$ and $\theta = 0.7$). (a) Phase space; (b) Poincaré section; (c) Lyapunov spectrum using the algorithm due to Wolf et al. [36]; (d) Lyapunov exponent using the algorithm due to Kantz [20]; (e) 0–1 test: *K*-metrics; (f) 0–1 test: *p*–*q* dynamics.

$\Delta t = 2\pi/200$. Two different simulations are performed considering $\theta = 0.7$ and different forcing amplitudes: periodic ($\delta = 0.038$) and chaotic ($\delta = 0.06$). Fig. 3 shows results related to periodic motion while Fig. 4 presents results of chaotic behavior. Basically, phase space, Poincare map, Lyapunov exponents evaluated with the algorithms due to Wolf et al. [36] and due to Kantz [20], and results of the 0–1 test considering *K* metrics for different values of *c* and the *p*–*q* space are shown in these pictures.

Periodic behavior (Fig. 3) has a closed curve on phase space and a Poincaré section with three points. Lyapunov exponent estimation using Wolf et al. algorithm shows that all values are negative. By employing the Kantz algorithm, a null slope is obtained considering a time delay 9.3 and embedding dimension 3. The 0–1 test shows that each metric has different behavior that is dependent to the value of *c* (Fig. 3e). This shows the importance to evaluate different values of *c* to obtain a proper median value of *K*. It is also noticeable the resonant-like phenomenon for some values of *c*. Besides, K_c and K_c^*, both calculated from the correlation method, present less influence with smaller variation under this resonant condition. The median value of *K* is close to zero characterizing a regular dynamics. The analysis of *p*–*q* dynamics shows closed curves with different amplitudes depending on the value of *c*.

Chaotic behavior (Fig. 4) shows a typical open orbit on phase space and a Poincaré section with strange attractor characteristic. The calculation of Lyapunov exponents using both the Wolf et al.

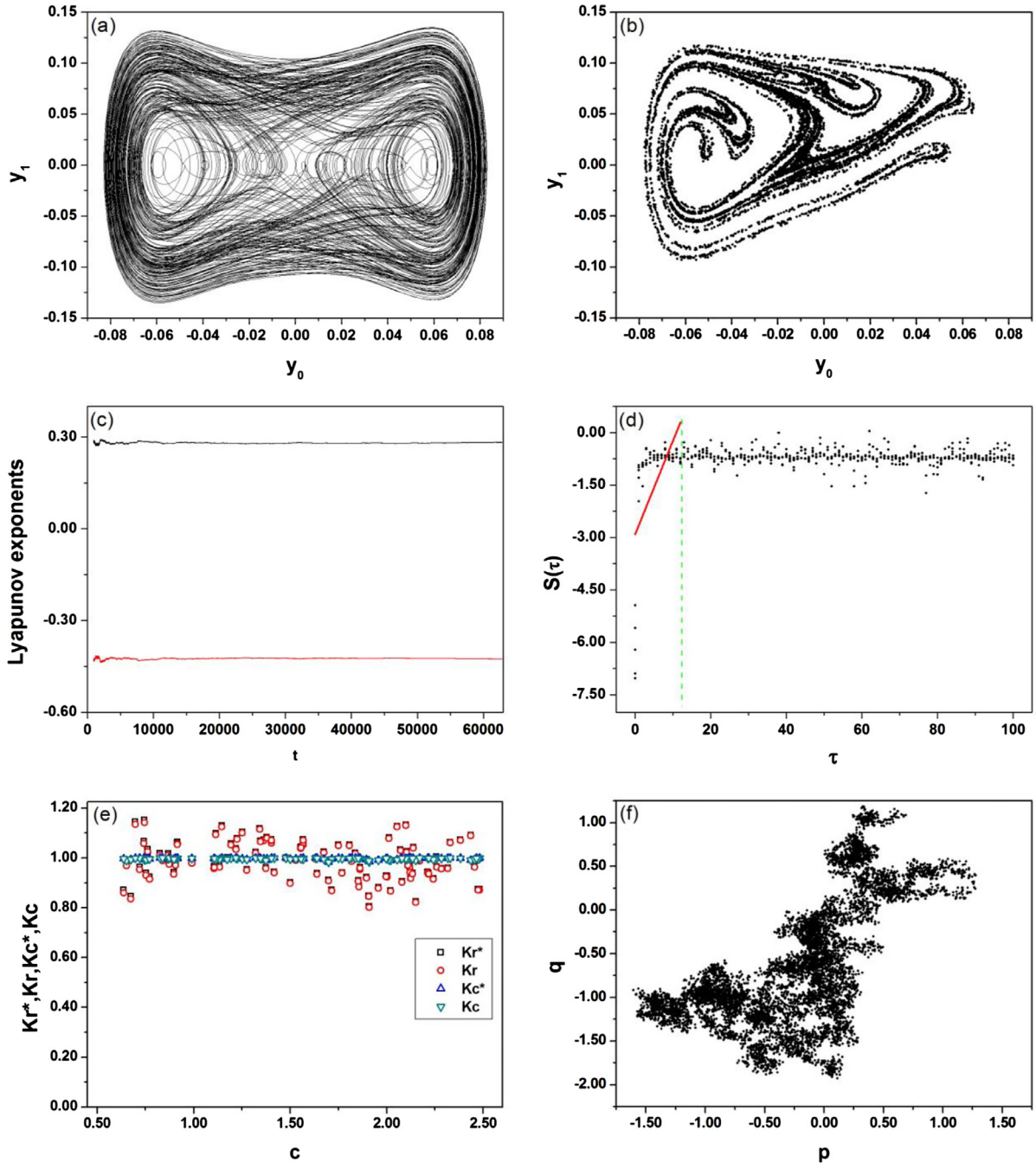

Fig. 4. Polynomial model - chaotic motion ($\delta = 0.06$ and $\theta = 0.7$). (a) Phase space; (b) Poincaré section; (c) Lyapunov spectrum using the algorithm due to Wolf et al. [36]; (d) Lyapunov exponent using the algorithm due to Kantz [20]; (e) 0–1 test: *K*-metrics; (f) 0–1 test: p–q dynamics.

and the Kantz algorithms presents positive values. The estimation of the Lyapunov exponent using Kantz algorithm needs to define the region related to horizontal trend. Fig. 4d shows a dashed line that represents this region. The estimation of the exponent is done by establishing the slope of the initial region considering a linear fit by least square method. In addition, the following parameters are adopted: time delay 9.3, embedding dimension 3 and length scale to search neighbors varies from 10^{-2} to 10^{-3}. The 0–1 test presents a distribution without resonant-like region and, in general, all metrics are similar for different values of c, except for K_r that shows a larger dispersion around the median value. The median value of K is close to 1 characterizing chaos. The p–q dynamics has an irregular unbounded behavior as observed in Fig. 4f. Table 3 summarizes the main results related to periodic and chaotic responses.

4. SMA model with internal constraints

The constitutive model with internal constraints was proposed by Paiva et al. [27] being able to capture the general thermomechanical behavior of SMAs, matching experimental data. This model considers different material properties and four macroscopic phases for the description of the SMA behavior. Besides strain, ε, and temperature, T, the model considers four more state variables associated with the volume fraction of each macroscopic phase, $\beta_i \in [0,1]$: β_1, associated with tensile detwinned martensite; β_2, related to compressive detwinned martensite; β_3, represents austen-

Table 3
Comparative analysis of diagnostic tools for 1-dof polynomial model.

Behavior	Lyapunov spectrum Wolf et al. [36]	Lyapunov exponent Kantz [20]	0–1 Test median values			
			K_r	K_c	K_r^*	K_c^*
Periodic	(0, −0.07,−0.07)	0.00	−0.0085	−0.0027	−0.0085	−0.0023
Chaotic	(+0.28, 0, −0.42)	0.26	0.9827	0.9981	0.9873	0.9981

ite; and β_4 corresponds to twinned martensite. Since there are restrictions related to phase coexistence, it is possible to use only three volume fractions: $\beta_4 = 1 - \beta_1 - \beta_2 - \beta_3$. Savi et al. [30] describes an SMA oscillator where the restitution force is described by this model. The dimensionless equations of motion has the following form:

$$\dot{y}_0 = y_1 \tag{10}$$

$$\dot{y}_1 = \delta \sin(\varpi t) - \xi y_1 - \mu_E y_0 - (\bar{\alpha} + \mu_E \alpha_h)(\beta_2 - \beta_1) + \mu_\Omega \bar{\Omega}_M (\theta - \theta_0) \tag{11}$$

$$\dot{\beta}_1 = \frac{1}{\mu_{\omega_0}\eta}\left\{\bar{\alpha} y_0 + \bar{\Lambda} + \left(2\bar{\alpha}\alpha_h + \mu_E \alpha_h^2\right)(\beta_2 - \beta_1) + \alpha_h\left[\mu_E y_0 - \mu_\Omega \bar{\Omega}_M (\theta - \theta_0)\right] - \kappa_{\pi 1}\right\} + \kappa_{x1} \tag{12}$$

$$\dot{\beta}_2 = \frac{1}{\mu_{\omega_0}\eta}\{-\bar{\alpha} y_0 + \bar{\Lambda} + (2\bar{\alpha}\alpha_h + \mu_E \alpha_h^2)(\beta_2 - \beta_1) - \alpha_h[\mu_E y_0 - \mu_\Omega \bar{\Omega}_M (\theta - \theta_0)] - \kappa_{\pi 2}\} + \kappa_{x2} \tag{13}$$

$$\dot{\beta}_3 = \frac{1}{\mu_{\omega_0}\eta_3}\left\{-\frac{1}{2}(\mu_{E_A} - 1)[y_0 + \alpha_h(\beta_2 - \beta_1)]^2 + \bar{\Lambda}_3 + (\bar{\Omega}_A - \bar{\Omega}_M)(\theta - \theta_0)[y_0 + \alpha_h(\beta_2 - \beta_1)] - \kappa_{\pi 3}\right\} + \kappa_{x3} \tag{14}$$

where δ and ϖ are excitation parameters; ξ is related to dissipation; θ represents the temperature; $\bar{\alpha}$, α_h, $\bar{\Omega}_A$, $\bar{\Omega}_M$, μ_E, μ_{E_A}, μ_Ω, μ_ω, η, η_3, $\bar{\Lambda}$, $\bar{\Lambda}_3$ are SMA parameters. It is important to observe that:

$$\mu_E = \frac{E}{E_M} = 1 + \beta_3\left(\mu_{E_A} - 1\right);\ \ \mu_{E_A} = \frac{E_A}{E_M}$$
$$\mu_\Omega = \frac{\Omega}{\Omega_M} = 1 + \beta_3\left(\mu_{\Omega_A} - 1\right);\ \ \mu_{\Omega_A} = \frac{\Omega_A}{\Omega_M} \tag{15}$$
$$\mu_{\omega_0} = \frac{\omega_0}{E_M};\ \ \omega_0 = \sqrt{\frac{E_M A}{ml}}$$

And that these parameters are related to constitutive parameters presented in Paiva et al. [27] as follows:

$$\bar{\alpha} = \frac{\alpha}{E_M}$$
$$\bar{\Omega}_M = \frac{\Omega_M T_M}{E_M};\ \ \bar{\Omega}_A = \frac{\Omega_A T_M}{E_M} \tag{16}$$
$$\bar{\Lambda} = \frac{\Lambda(T)}{E_M};\ \ \bar{\Lambda}_3 = \frac{\Lambda_3(T)}{E_M}$$

Concerning the phase transformation stress definitions, temperature dependent relations are adopted:

$$\bar{\Lambda} = \begin{cases} -L_0 + L(\theta - 1), & if\ \theta > 1 \\ -L_0, & if\ \theta \le 1 \end{cases} \tag{17}$$

$$\bar{\Lambda}_3 = \begin{cases} -L_0^A + L^A(\theta - 1), & if\ \theta > 1 \\ -L_0^A, & if\ \theta \le 1 \end{cases} \tag{18}$$

Table 4
Parameters of the internal constraints model.

Parameter	Value	Parameter	Value
μ_{E_A}	1.2857	L_0	3.57×10^{-6}
μ_{Ω_A}	4.3529	L	988×10^{-6}
μ_{ω_0}	96.61×10^{-9}	L_0^A	15×10^{-6}
$\bar{\alpha}$	3.57×10^{-3}	L^A	4.4×10^{-3}
α_h	0.0519	$\bar{\Omega}_A$	5.13×10^{-3}
$\eta^L = \eta_3^L$	1.0×10^7	$\bar{\Omega}_M$	1.18×10^{-3}
$\eta^U = \eta_3^U$	2.7×10^7		

In addition, it is important to observe internal constraints that establish proper phase transformation descriptions. In general, this is controlled by indicator functions related to convex sets. The terms $\kappa_\pi = (\kappa_{\pi 1}, \kappa_{\pi 2}, \kappa_{\pi 3})$ and $\kappa_\chi = (\kappa_{\chi 1}, \kappa_{\chi 2}, \kappa_{\chi 3})$ represent projections to the respective convex set. They can be understood as sub-differentials of the indicator function or Lagrange multipliers. For more details, please refer to Paiva et al. [27] and Savi et al. [30].

Numerical simulations are carried out considering the operator split technique allowing one to treat the coupled system as decoupled problems where classical procedures can be used for numerical integration. An iterative procedure combines the fourth order Runge-Kutta method, related to dynamical space (displacement-velocity), with the projection algorithm [27], associated with the constitutive equations. For $\beta_n (n = 1, 2, 3)$ calculation, the evolution equations are solved using an iterative implicit Euler method. Time steps smaller than $2\pi/2000\varpi$ are adopted. Typical dynamical parameters are considered: $\xi = 5 \times 10^{-6}$ and $\varpi = 1$. Besides, forcing amplitude, δ is varied in order to define the system behavior. In all simulations, it is assumed the value $\theta = \theta_0 = 0.99$. Table 4 presents other physical properties related to SMA. It is important to observe that dissipation parameters, η and η_3, are adopted with different values for loading ($\eta^L$and η_3^L) and unloading ($\eta^U$and η_3^U).

Two kinds of behaviors are of concern considering different forcing amplitudes: periodic ($\delta = 3 \times 10^{-3}$) and chaotic ($\delta = 6 \times 10^{-3}$). Fig. 5 shows the periodic behavior while Fig. 6 shows chaotic behavior.

Fig. 5 presents phase space with a closed curve and a Poincaré section associated with a single point, characterizing a period-1 response. Kantz algorithm has a null slope using a time delay 4×10^{-3} and embedding dimension 3. Once again, it is noticeable the influence of c value on the K estimation, which the median value is close to zero. Besides, the p–q dynamics are related to closed curves associated with different amplitudes. Two values of c are presented: $c = 2.308$ (appropriate value); $c = 1.582$ (resonant-like region). Note that, in essence, both behaviors are similar since they are associated with closed curves.

Fig. 6 shows the same set of curves for the chaotic behavior. Phase space and Poincaré section present typical chaotic characteristics. Results related to Lyapunov exponents and 0–1 test are also assuring the chaotic response. Kantz algorithm presents a curve with a slope associated with $\lambda = 0.24$. This result is obtained using a time delay 8×10^{-3} and an embedding dimension 3. The 0–1 test presents a value close to 1 being associated with an irregular p–q

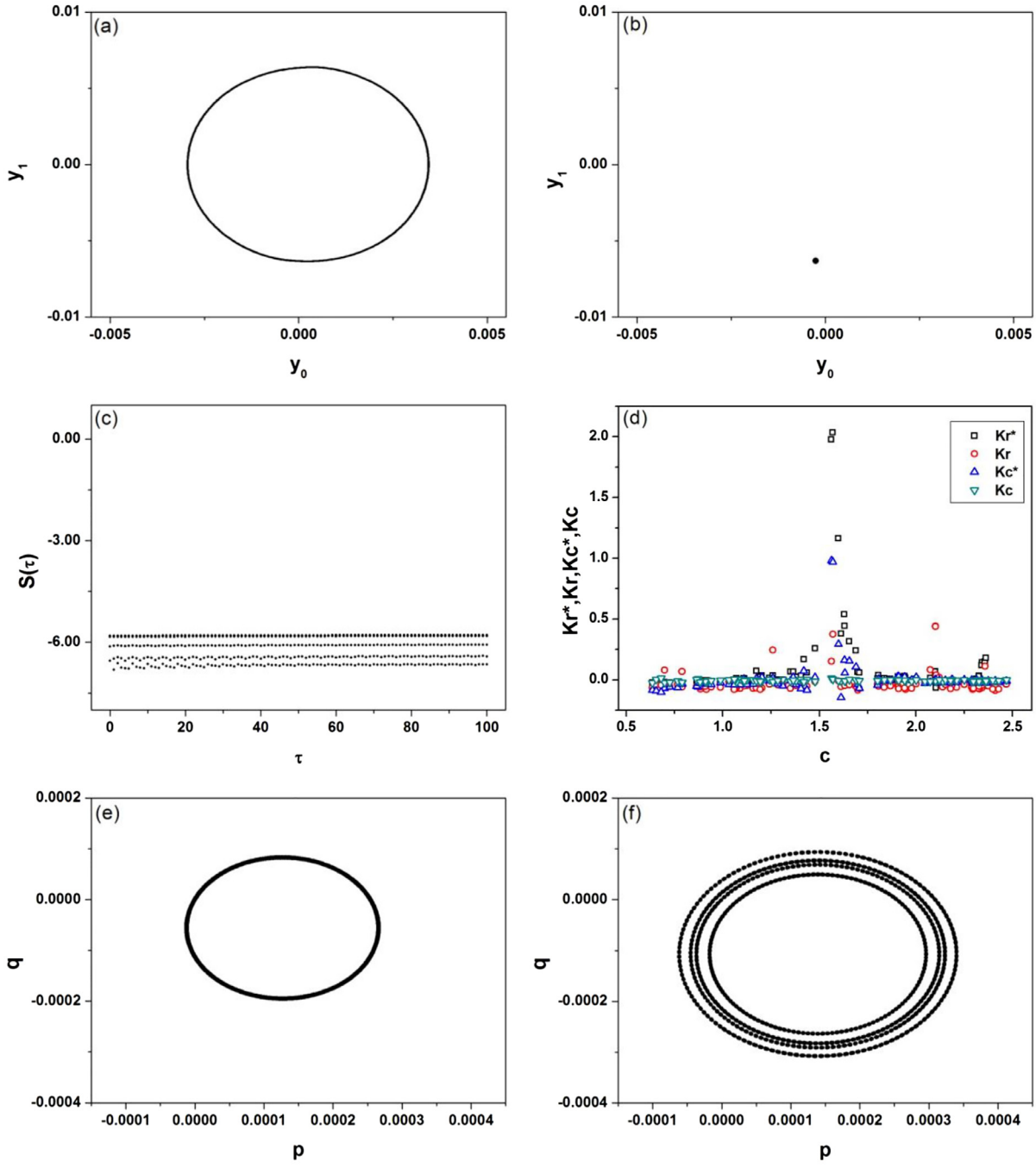

Fig. 5. Model with internal constraints - periodic motion. (a) Phase space; (b) Poincaré section; (c) Lyapunov exponent using the algorithm due to Kantz [20]; (d) 0–1 test: K-metrics; (e) 0–1 test: p–q dynamics ($c = 2.308$); (f) 0–1 test: p–q dynamics ($c = 1.582$).

Table 5
Comparative analysis of diagnostic tools for the model with internal constraints.

Behavior	Lyapunov exponent Kantz	0–1 test median values			
		K_r	K_c	K_r^*	K_c^*
Periodic	0.00	−0.0511	−0.0059	0.0002	−0.0128
Chaotic	0.19	0.8127	0.9947	0.9491	0.9981

dynamics. The analysis of different values of parameter c shows that K-metrics does not show the resonant-like phenomenon but shows a dispersion of the regression metrics, K_r^* and K_r, around the median value. Results of both periodic and chaotic motions are summarized in Table 5.

5. SMA Bernardini–Pence's model

The Bernardini–Pence's thermomechanical constitutive model for SMAs has been adapted in Bernardini and Rega [4] as a model for the restoring force of SMA devices suitable for the use in the

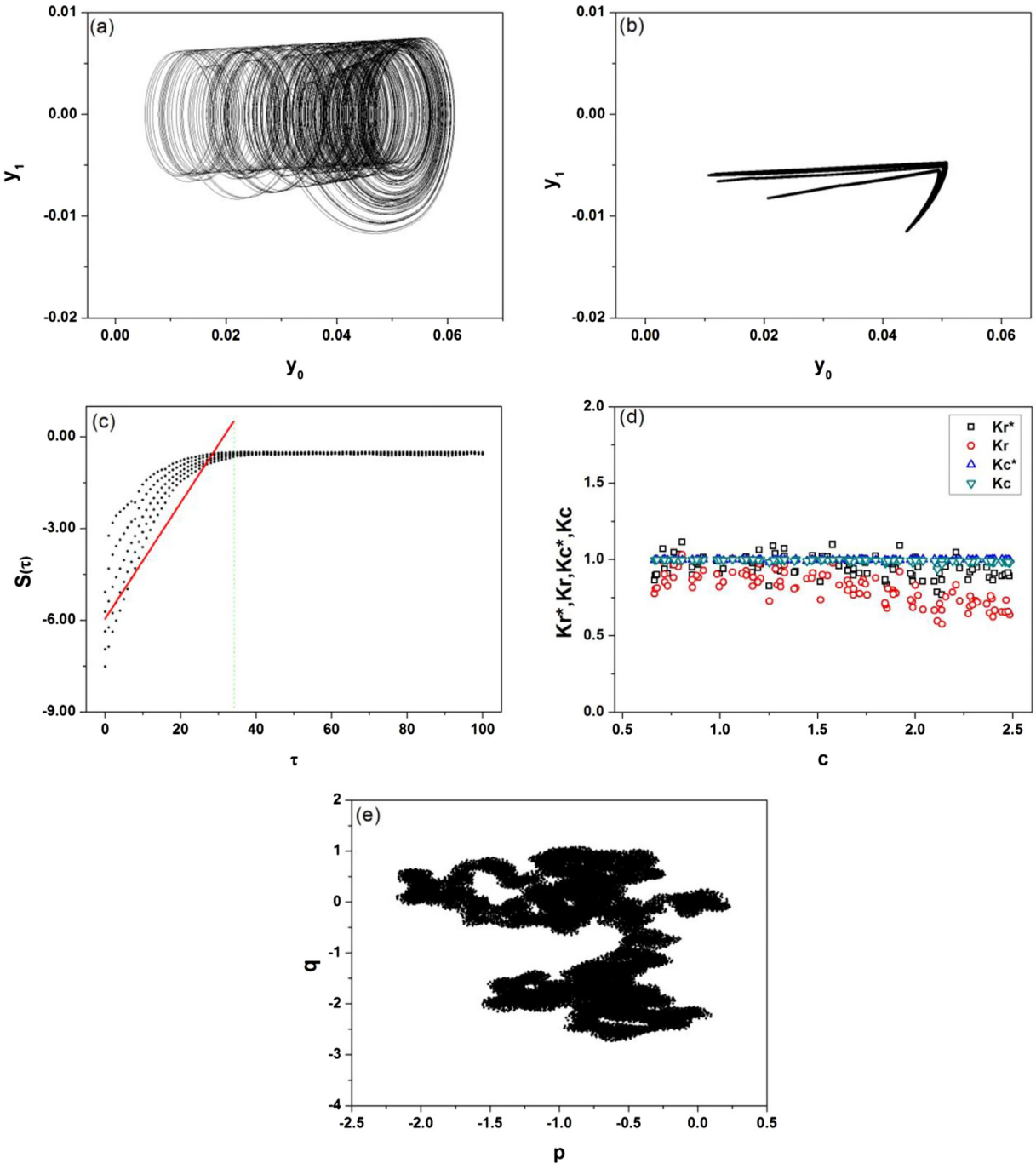

Fig. 6. Model with internal constraints - chaotic motion. (a) Phase space; (b) Poincaré section; (c) Lyapunov exponent using the algorithm due to Kantz [20]; (d) 0–1 test: *K*-metrics; (e) 0–1 test: *p*–*q* dynamics.

analysis of nonlinear dynamics of Shape Memory Oscillators (SMO) [3].

The model, as presented in this work, is expressed in terms of dimensionless variables and model parameters. Specifically, quantities with the dimensions of temperature are normalized with respect to a reference value θ_{ref}, greater than the transformation temperature A_f, whereas those with the dimensions of length and force are normalized, respectively, to the displacement u_{Ms} and force f_{Ms} at the beginning of the forward A→M transformation at the temperature θ_{ref}. θ_e is the environment dimensionless temperature.

The state of the SMO is described by dimensionless variables: displacement, y_0, velocity, y_1, temperature, θ, and martensitic volume fraction, $\beta \in [0,1]$. Moreover, in order to model the complex hysteretic behavior of SMA that produces internal subloops, the state of the device depends also the value β_0 of the martensitic fraction β attained at the beginning of the last phase transformation occurred before time t. As discussed in Bernardini and Rega [4], the generally non-isothermal, time evolution of the SMO is described by the following system of differential equations:

$$\dot{\boldsymbol{y}}_0 = \boldsymbol{y}_1 \tag{19}$$

$$\dot{\boldsymbol{y}}_1 = \boldsymbol{\delta}\,\mathbf{sin}(\boldsymbol{\varpi t}) - \boldsymbol{y}_0 - \boldsymbol{\xi y}_1 - \boldsymbol{\lambda}\mathbf{sign}(\boldsymbol{y}_0)\boldsymbol{\beta} \tag{20}$$

$$\dot{\boldsymbol{\beta}} = \boldsymbol{Z}[\mathbf{sign}(\mathbf{y_0})\mathbf{y_1} - \mathbf{JQ}] \tag{21}$$

$$\dot{\boldsymbol{\theta}} = \boldsymbol{ZL}\left(\frac{\boldsymbol{\Lambda}}{\boldsymbol{J\lambda}} + \boldsymbol{\theta}\right)[\mathbf{sign}(\mathbf{y_0})\mathbf{y_1} - \mathbf{JQ}] + \boldsymbol{Q} \tag{22}$$

where $\mathrm{sign}(x)=x/|x|$ and $Q = h(\theta - \theta_e)$ is the rate of heat exchanged with environment by convection, depending on the coefficient of heat transfer h.

The constitutive functions Λ and Z take different expressions depending on the fulfillment of suitable transformation criteria that detect the occurrence of the two-phase transformations [4]. Subscripts F and R indicate, respectively, the expressions relative to the Forward (A→M), upper plateaus, and Reverse (M→A), lower plateaus, transformations:

$$\begin{aligned}
\Lambda_F(\beta,\beta_0) &= \lambda\frac{(J-1)(q_2-1)}{2} + \lambda(J-1)(1-q_1)\Psi_F(\beta,\beta_0)\\
\Lambda_R(\beta,\beta_0) &= -\lambda\frac{(J-1)(q_2-1)}{2}\\
&\quad -\lambda(J-1)q_2(1-q_3)\Psi_R(\beta,\beta_0)\\
Z_{F,R}(\theta,\beta,\beta_0) &= \frac{1}{\lambda + JL\vartheta + \frac{L}{\lambda}\Lambda_{F,R} + \frac{1}{\lambda}\frac{\partial\Lambda_{F,R}}{\partial\beta}}
\end{aligned} \tag{23}$$

where $\Psi_{F,R}$ are constitutive functions that determine the shape of the upper/lower pseudoelastic plateaus and q_1, q_2, q_3 and the other quantities are model parameters. Whereas various choices at different levels of refinement are possible the following one is adopted,

$$\Psi_F(\beta,\beta_0) = \frac{1}{2}\left(1 + \frac{1}{b}\ln\frac{1-\beta+e^b(\beta-\beta_0)}{\beta-\beta_0+e^b(1-\beta)}\right) \tag{24}$$

$$\Psi_R(\beta,\beta_0) = \frac{1}{2}\left(-1 + \frac{1}{b}\ln\frac{\beta-\beta_0+e^b\beta}{-\beta+e^b(\beta-\beta_0)}\right) \tag{25}$$

Here b is a parameter that determines the smoothness of the transition between the elastic branch and the transformation plateaus.

The second law of thermodynamics expresses the non-negativity of the rate of energy dissipation Γ. In this framework, $\Gamma = \Lambda\dot{\beta}$. Since $\Lambda = \Lambda_F$ when $\dot{\beta} > 0$and $\Lambda = \Lambda_R$ when $\dot{\beta} < 0$the second law requires: $\Lambda_F \geq 0$, $\Lambda_R \leq 0$. Such constraints impose limitations on the range of variations of model parameters. For example, evaluating Λ_F at the beginning of the upper plateau the following constraint among λ, J, q_2 is obtained:

$$\Lambda_F(0,0) = \lambda\frac{(J-1)(q_2-1)}{2} \geq 0 \tag{26}$$

Taking into account Eqs. (20) and (21), the system response depends on seven model parameters (q_1, q_2, q_3, λ, L, h, J), besides the above mentioned b.

The first four parameters determine the shape of the outer pseudoelastic loop. In particular: $q_1$and q_3 respectively influence the slopes of the isothermal upper and lower plateaus. Physically meaningful ranges of values may be identified with $q_1 \in$ [0.7, 1.0] and $q_3 \in$ [1.0, 1.5]. On the other hand, q_2 determines the position of the isothermal lower plateau with respect to the upper one hence determines the size of the hysteresis loop. Finally, λ directly influences the length of both plateaus. The remaining three parameters characterize the thermomechanical properties.

In particular, the thermal parameters (L, h) determine how much heat is produced or absorbed during mechanical loading (L) and the rate at which the involved heat can flow out from the system to the environment by convection (h). Physically meaningful ranges of values may be identified with $L \in$ [0.0, 0.5] and $h \in$ [0.0, 0.2]. The limit case $L = 0$ corresponds to SMAs whose transformations produce negligible amounts of heat, while the limit case $h = 0$ models an adiabatic environment in which all the heat produced remains in the system. The thermo-mechanical parameter J determines the slope of the linear dependence of the transformation forces on the temperature. A physically meaningful range of values may be identified with $J \in (1.0, 4.0]$.

Table 6
Parameters of the Bernardini–Pence's model.

q_1	q_2	q_3	λ
0.98	1.2	0.98	8.125
L	H	J	b
0.001	0.08	3.1742	0.03

Table 7
Comparative analysis of diagnostic tools for Bernardini–Pence's model.

Behavior	Lyapunov exponent Kantz	0–1 test median values			
		K_r	K_c	K_r^*	K_c^*
Periodic	0.00	−0.0064	0.0000	0.0055	0.0092
Chaotic	0.53	0.8668	0.9967	0. 9893	0.9981

Numerical integration of the equations of motion is performed with fourth order Runge-Kutta algorithm with 4000 steps per period. The output is then sampled to get time series of 200,000 points. Model parameters are fixed to the following values in Table 6. This choice of parameters corresponds to a device with a hysteresis loop of medium-high size and low hardening. The latent heat of transformation is low so that thermal phenomenon is small and the resulting conditions are close to the isothermal ones [3,4].

Two distinct behaviors are treated in order to evaluate the 0–1 test: periodic ($\delta = 1$; $\varpi = 0.4$) and chaotic ($\delta = 1$; $\varpi = 0.227$). Figs. 7 and 8 present the analysis showing phase space, Poincaré section, Lyapunov exponent, 0–1 test results in form of K-metrics and p–q dynamics.

Fig. 7 presents periodic response showing a closed curve on phase space and a Poincaré section related to a small region, essentially related to a single point. Lyapunov exponent is estimated from the Kantz algorithm using a time delay 1.2×10^{-2} and an embedding dimension 5, presenting a null slope assuring the conclusion about periodicity. The 0–1 test presents a K-metrics distributed over the region close to zero for all values of c parameter. The p–q dynamics has a closed curve, characteristic of periodic motion.

Fig. 8 presents chaotic response. Typical phase space and Poincaré sections are identified. Lyapunov exponent is estimated from the Kantz algorithm using a time delay 1.2×10^{-2} and an embedding dimension 5, being related to a positive slope confirming the conclusion. The 0–1 test presents a K-metrics with sparse distribution of all K-metrics, except for K_c^* that is distributed close to 1. The median values, however, are all close to 1. The p–q dynamics is irregular and unbounded. Table 7 summarizes all results related to both periodic and chaotic motions.

6. SMA polynomial model – two-degree of freedom system

A two-degree of freedom oscillator (2-dof) presented in Fig. 1b is now analyzed in order to treat a dynamical system with higher dimension. Shape memory behavior is described by considering a polynomial constitutive model. Dimensionless displacements (y_0 and y_2) and velocities (y_1 and y_3) are employed to obtain equations of motion [24,31]:

$$\begin{aligned}
\dot{y}_0 &= y_1\\
\dot{y}_1 &= \delta_1\sin(\varpi_1\tau) - (\xi_1 + \xi_2\vartheta_{21}\mu)y_1 + \xi_2\vartheta_{21}\mu y_3
\end{aligned}$$

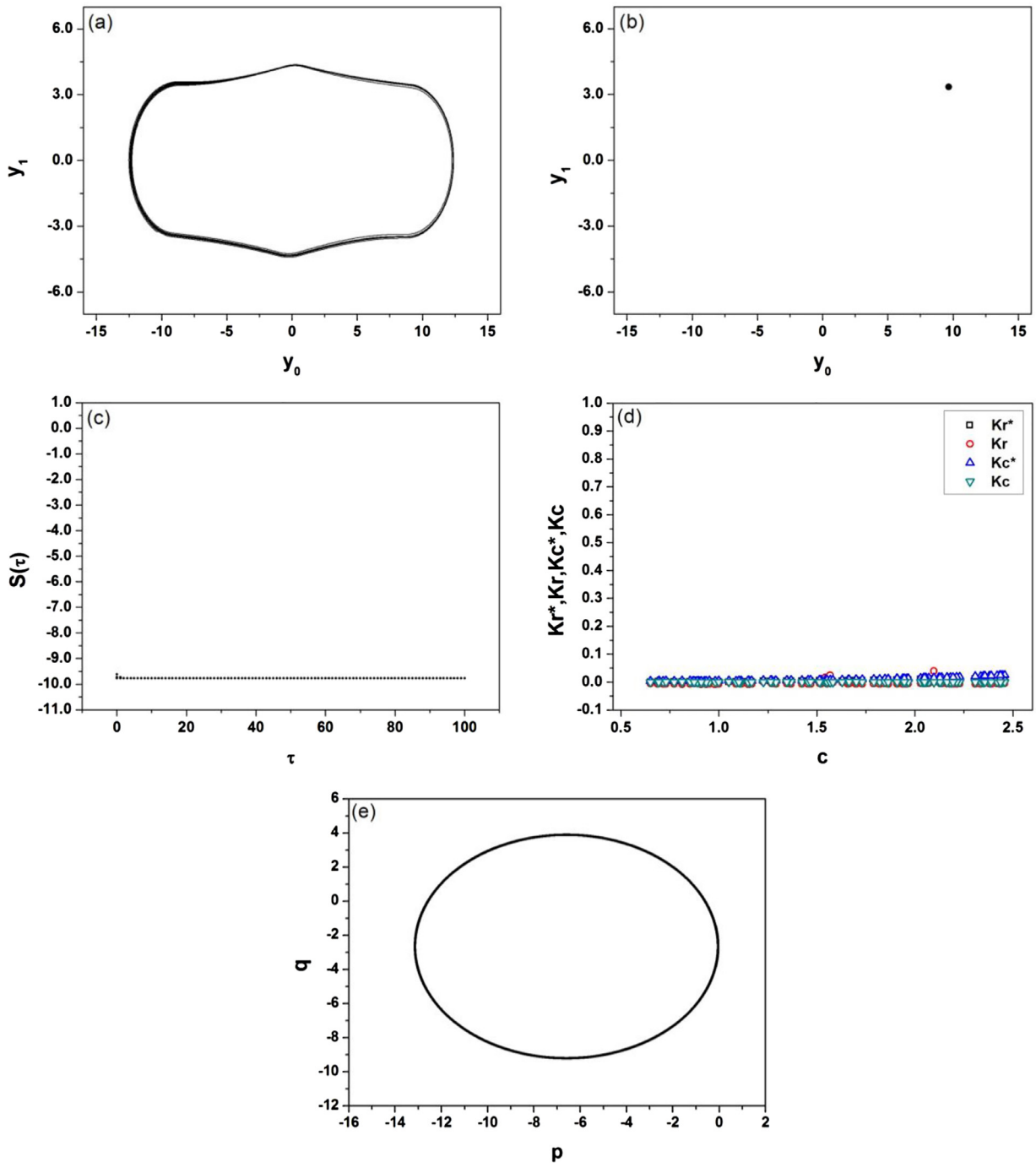

Fig. 7. Bernardini–Pence's model - periodic motion. (a) Phase space projections; (b) Poincaré section projections; (c) Lyapunov exponent using the algorithm due to Kantz [20]; (d) 0–1 test: *K*-metrics; (e) 0–1 test: *p*–*q* dynamics.

$$
\begin{aligned}
&-[(\theta_1-1)+\vartheta_{21}^2\mu(\theta_2-1)]y_0+\vartheta_{21}^2\mu(\theta_2-1)y_2\\
&+\phi_1 y_0^3-\gamma_1 y_0^5-\phi_2\vartheta_{21}^2\mu(y_2-y_0)^3+\gamma_2\vartheta_{21}^2\mu(y_2-y_0)^5\\
\dot{y}_2 &= y_3\\
\dot{y}_3 &= \alpha_{21}^2\delta_2\sin(\varpi_2\tau)+\xi_2\vartheta_{21}y_1-(\xi_2\alpha_{21}+\xi_3\vartheta_{21}\alpha_{32})y_3\\
&+\vartheta_{21}^2(\theta_2-1)y_o-\left[\vartheta_{21}^2(\theta_2-1)+\vartheta_{21}^2\vartheta_{32}^2(\theta_3-1)\right]y_2\\
&+\phi_2\vartheta_{21}^2(y_2-y_0)^3-\gamma_2\vartheta_{21}^2(y_2-y_0)^5+\phi_3\vartheta_{21}^2\vartheta_{32}^2y_2^3\\
&-\gamma_3\vartheta_{21}^2\vartheta_{32}^2y_2^5
\end{aligned}
\tag{27}
$$

where δ_1, δ_2, ϖ_1 and ϖ_1 are excitation parameters; ξ_1, ξ_2 and ξ_3 are the viscous dissipation parameters; μ is related to mass relation; ϑ_{21}, ϑ_{32}, ϕ_1, ϕ_2, ϕ_3, γ_1, γ_2 and γ_3 are parameters related to SMA properties.

Numerical simulations are performed by employing a fourth-order Runge-Kutta scheme with time steps smaller than $\Delta t = 2\pi/200$. Table 8 presents the system parameters employed in all simulations [24]. Besides, forcing amplitudes, δ_i, and temperature, θ_i, are varied in order to define the system behavior.

Four distinct kinds of behaviors are of concern varying forcing amplitudes and SMA temperatures: periodic ($\delta_1=0.06$, $\delta_2=0$; $\theta_1=\theta_3=0.7$, $\theta_2=3.5$); quasi-periodic ($\delta_1=0.06$, $\delta_2=0$; $\theta_1=\theta_3=1.5$, $\theta_2=3.5$); chaotic ($\delta_1=0.06$, $\delta_2=0$; $\theta_1=\theta_2=\theta_3=0.7$); hyperchaotic ($\delta_1=0.06$, $\delta_2=0$; $\theta_1=\theta_3=0.7$,

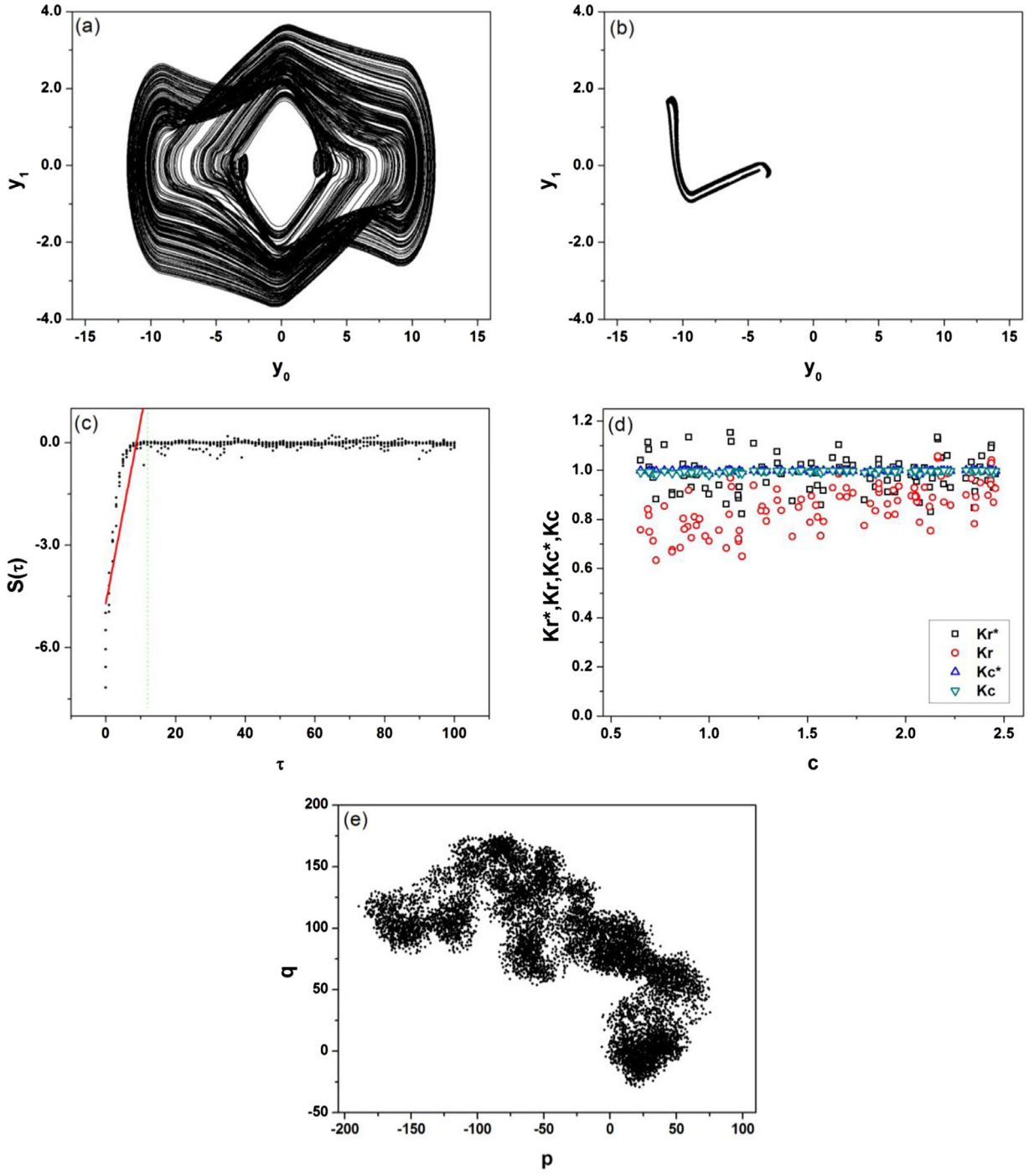

Fig. 8. Bernardini–Pence's model - chaotic motion. (a) Phase space projections; (b) Poincaré section projections; (c) Lyapunov exponent using the algorithm due to Kantz [20]; (d) 0–1 test: *K*-metrics; (e) 0–1 test: *p*–*q* dynamics.

Table 8
Parameters of the 2-dof polynomial model.

Parameter	Value	Parameter	Value
$\varpi_1 = \varpi_2$	1.0	$\gamma_1 = \gamma_2 = \gamma_3$	4.7×105
$\xi_1 = \xi_2 = \xi_3$	0.2	$\vartheta_{21} = \vartheta_{32}$	1.0
$\phi_1 = \phi_2 = \phi_3$	1.3×103	μ	1.0

$\theta_2 = 1.5$). Figs. 9 to 12 present results related to the 2-dof SMA system. Results are presented as subspaces of the original state space, related to each one of the masses.

Fig. 9 shows the periodic behavior associated with a closed curve and a single point on Poincaré section. Lyapunov spectrum does not present positive values. Kantz algorithm has a null slope using a time delay 0.3 and embedding dimension 5. The 0–1 test presents values close to zero. Concerning *p*–*q* dynamics, a closed curve is obtained.

Fig. 10 shows the quasi-periodic behavior characterized by a closed curve on Poincaré section. The Lyapunov spectrum presents two null values and no other positive exponent. Kantz algorithm has slope close to zero using a time delay 0.279 and embedding dimension 5. The 0–1 test has a typical behavior presenting two

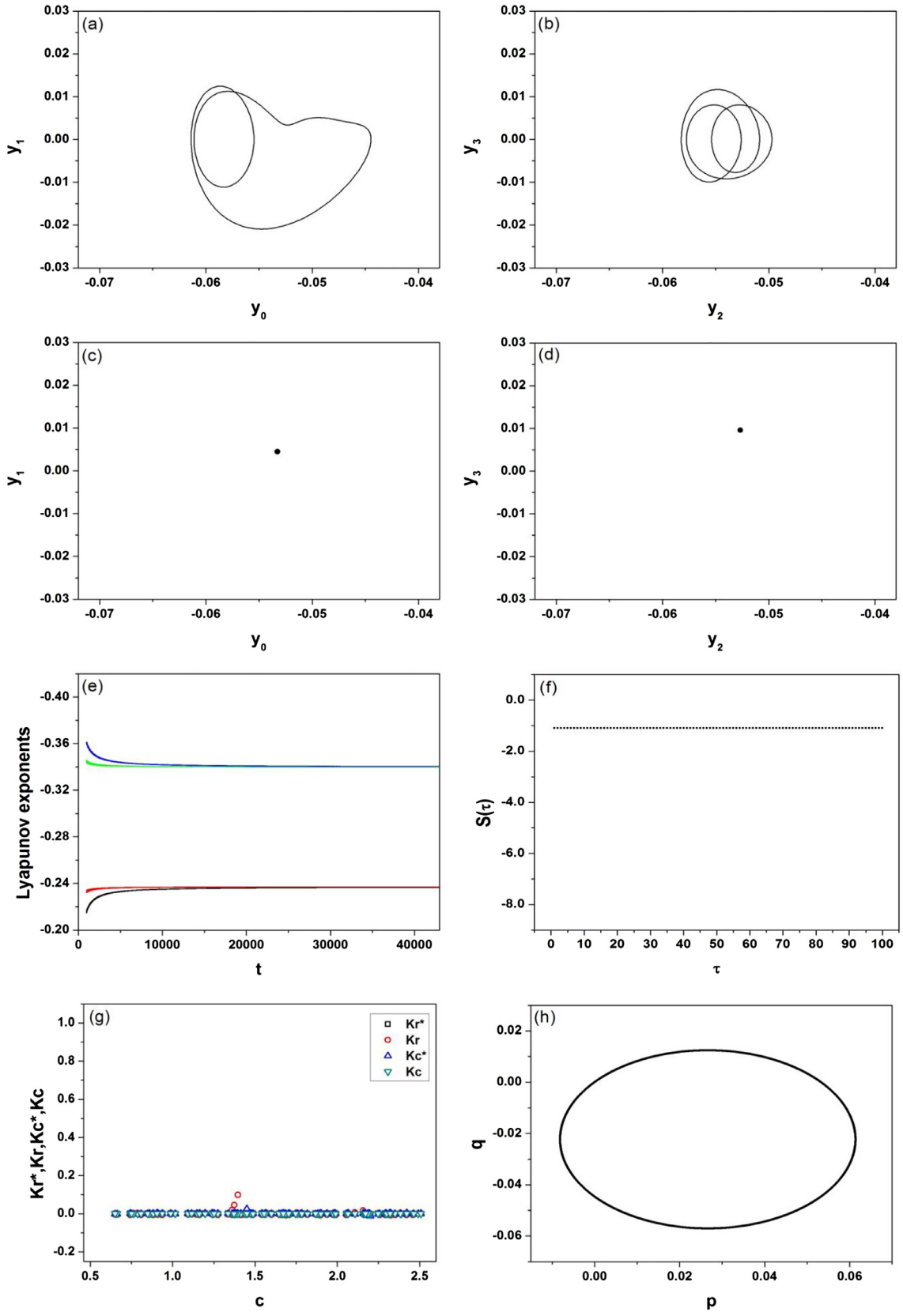

Fig. 9. Polynomial model with 2dof - periodic motion ($\delta_1 = 0.06$, $\delta_2 = 0$; $\theta_1 = \theta_3 = 0.7$, $\theta_2 = 3.5$). (a) Phase space projections; (b) Poincaré section projections; (c) Lyapunov spectrum using the algorithm due to Wolf et al. [36]; (d) Lyapunov exponent using the algorithm due to Kantz [20]; (e) 0–1 test: *K*-metrics; (f) 0–1 test: *p*–*q* dynamics.

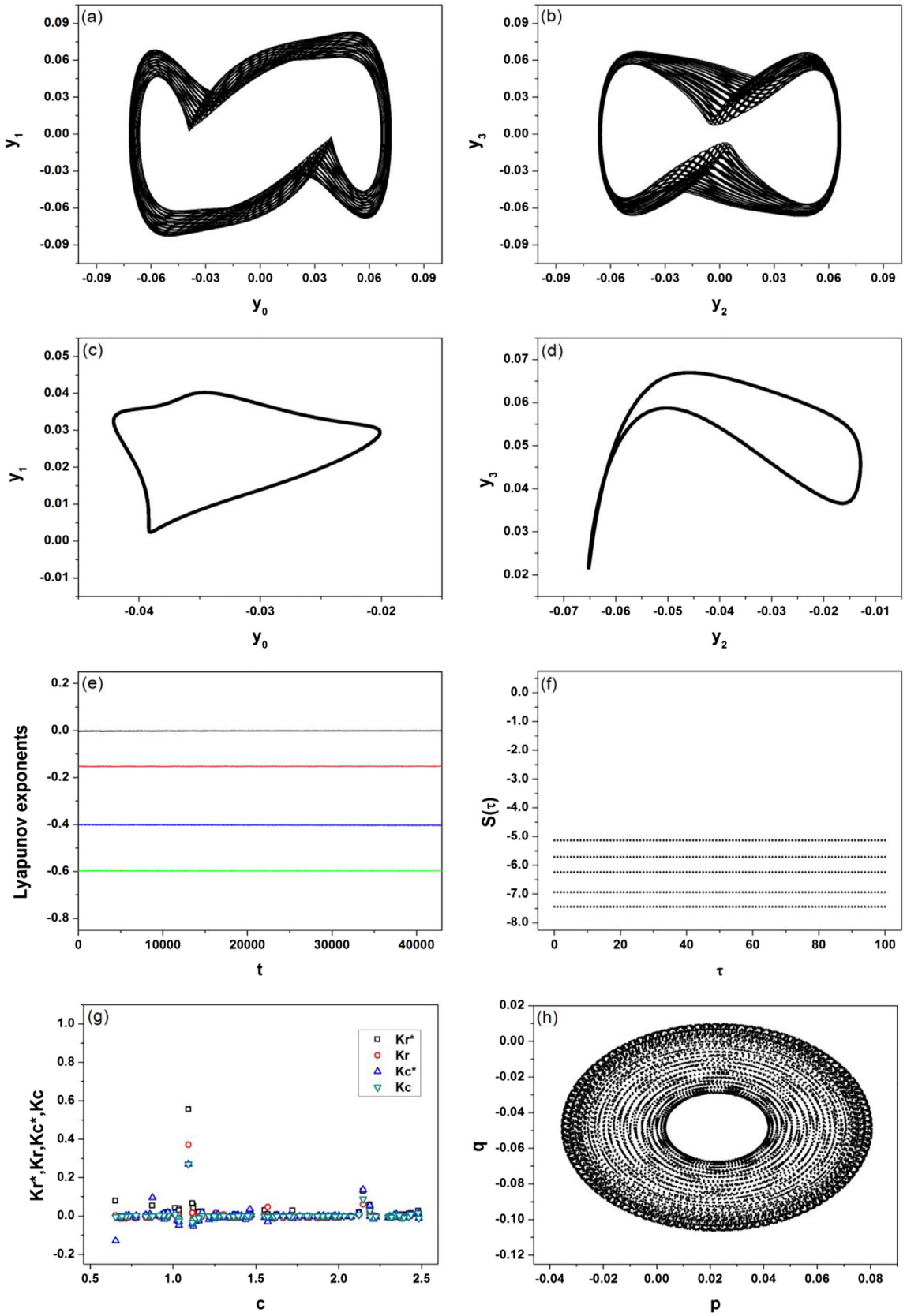

Fig. 10. Polynomial model with 2dof - quasi-periodic motion ($\delta_1 = 0.06$, $\delta_2 = 0$; $\theta_1 = \theta_3 = 1.5$, $\theta_2 = 3.5$). (a,b) Phase space projections; (c,d) Poincaré section projections; (e) Lyapunov spectrum using the algorithm due to Wolf et al. [36]; (f) Lyapunov exponent using the algorithm due to Kantz [20]; (g) 0–1 test: *K*-metrics; (h) 0–1 test: *p*–*q* dynamics.

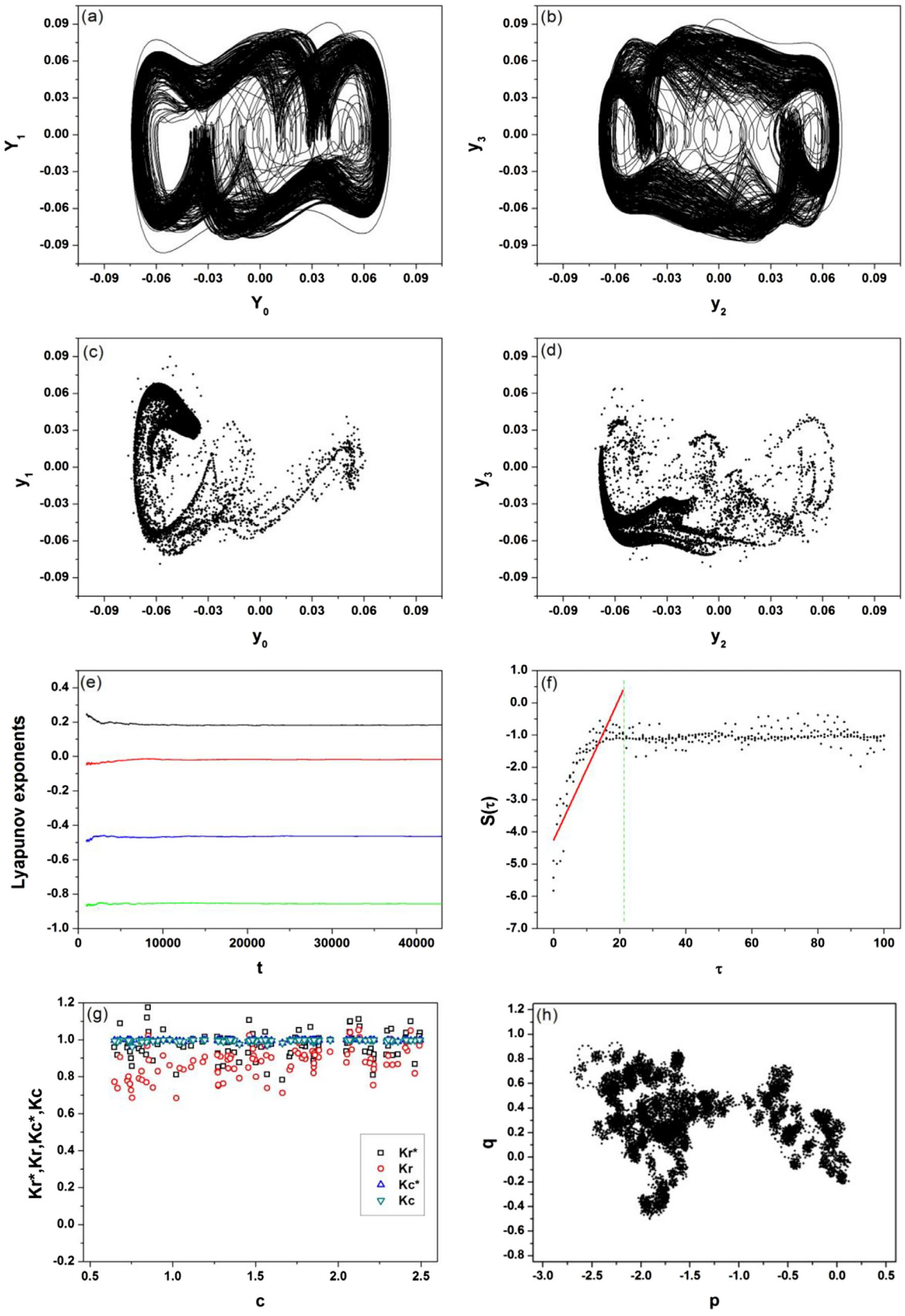

Fig. 11. Polynomial model with 2dof - chaotic motion ($\delta_1 = 0.06$, $\delta_2 = 0$; $\theta_1 = \theta_2 = \theta_3 = 0.7$). (a,b) Phase space projections; (c,d) Poincaré section projections; (e) Lyapunov spectrum using the algorithm due to Wolf et al. [36]; (f) Lyapunov exponent using the algorithm due to Kantz [20]; (g) 0–1 test: *K*-metrics; (h) 0–1 test: *p*–*q* dynamics.

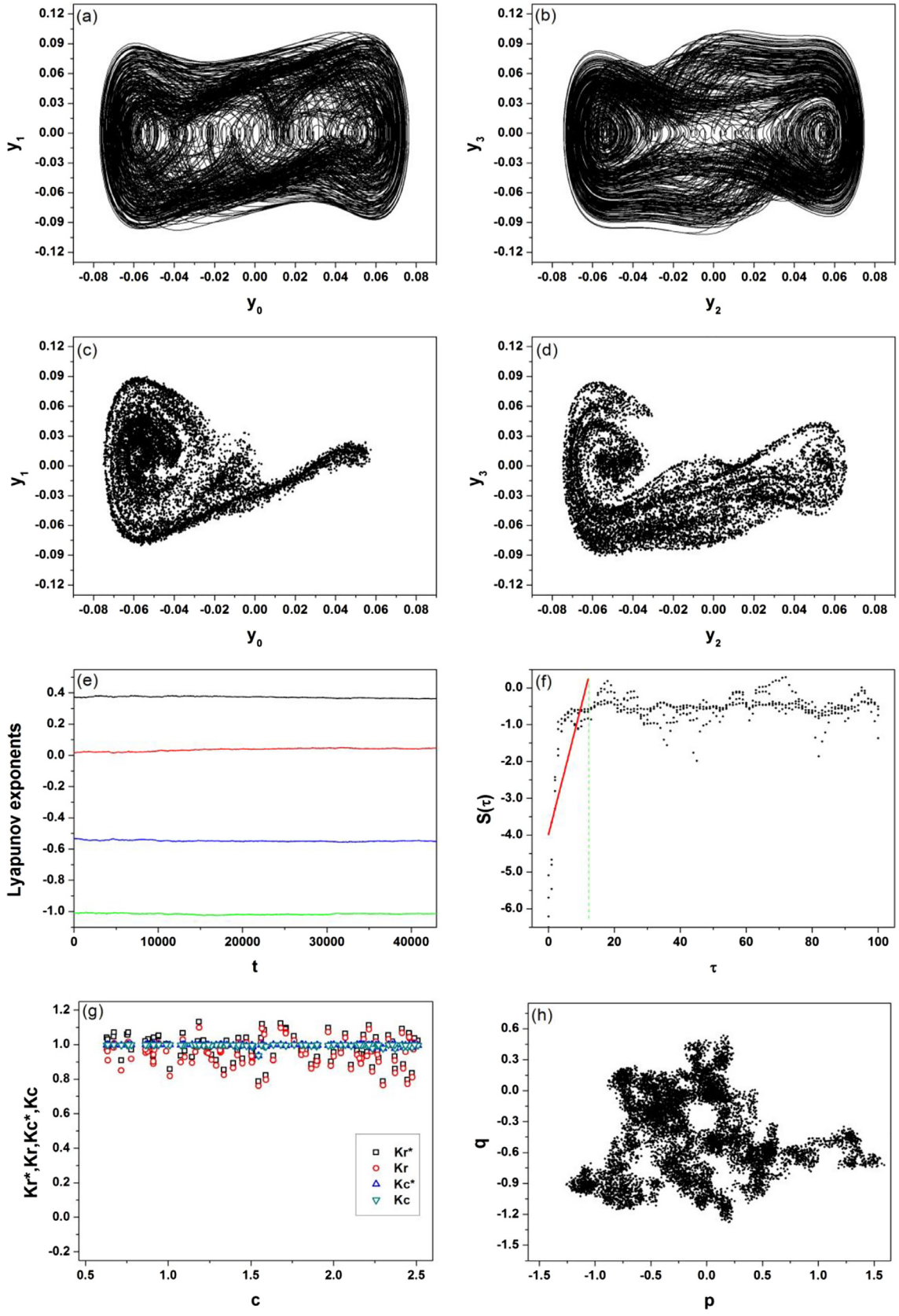

Fig. 12. Polynomial model with 2dof - hyperchaotic motion. $\delta_1 = 0.06$, $\delta_2 = 0$; $\theta_1 = \theta_3 = 0.7, \theta_2 = 1$. (a,b) Phase space projections; (c,d) Poincaré section projections; (e) Lyapunov spectrum using the algorithm due to Wolf et al. [36]; (f) Lyapunov exponent using the algorithm due to (1994); (g) 0–1 test: *K*-metrics; (h) 0–1 test: *p*–*q* dynamics.

Table 9
Comparative analysis of diagnostic tools for 2-dof system with polynomial model.

Behavior	Lyapunov spectrum Wolf et al.	Lyapunov exponent Kantz	0–1 Test median values			
			K_r	K_c	K_r^*	K_c^*
Periodic	(0, −0.25, −0.27, −0.29, −0.32)	0.00	0.0011	−0.0061	0.0018	−0.0003
Quasi-Periodic	(0, 0, −0.15, −0.40, −0.59)	0.00	−0.0079	−0.0014	−0.0014	−0.0027
Chaotic	(+0.19, 0, −0.02, −0.46, −0.86)	0.22	0.8906	0.9978	0.9729	0.9983
Hyperchaotic	(+0.36, +0.04, 0, −0.55, −1.01)	0.31	0.9536	0.9982	0.9842	0.9982

resonant points varying c parameter, but pointing for a value close to zero. The p–q dynamics is related to a closed curve. It should be pointed out that the difference between periodic and quasi-periodic motions can be defined only by the Lyapunov spectrum.

Fig. 11 shows the chaotic behavior characterized by a strange attractor on Poincaré section. Lyapunov spectrum has one positive value confirming the chaotic behavior. Kantz algorithm clearly presents a positive slope using a time delay 0.093 and embedding dimension 5. The 0–1 test gives a value close to 1, presenting a distribution over this value without a clear resonant behavior for c parameter. The p–q dynamics has an irregular distribution that points out a divergence towards an unbounded evolution, which is an indication of the occurrence of chaotic behavior.

Fig. 12 shows the hyperchaotic behavior. Lyapunov spectrum presents more than one positive value, representing two unstable directions. Kantz algorithm identify just the maximum value and presents a positive slope using a time delay 0.062 and embedding dimension 5. The 0–1 test presents response similar to chaos, with a value close to 1. The p–q dynamics has also the same characteristic of the chaotic behavior. It should be highlighted that the distinction between chaos and hyperchaos can only be done with the Lyapunov spectrum.

Table 9 summarizes results for the four kinds of behaviors. It shows Lyapunov exponents evaluated with the algorithms due to Wolf et al. [36] and due to Kantz [20], and also results of the different K-metrics of the 0–1 test.

7. Conclusions

This paper deals with the application of the 0–1 test to diagnose chaos in shape memory alloy systems. Time series are generated from equations of motion of single and two-degree of freedom oscillators where the restitution force is described by three different constitutive models. Basically, Poincaré map time series is employed. Lyapunov exponents are estimated by considering the algorithms due to Wolf et al. [36] and Kantz [20]. The 0–1 test is applied to all systems and compared with the Lyapunov exponents. Four different metrics of the test are employed: M-Regression, M-Correlation, D-Regression and D-Correlation. Four distinct kinds of behavior are discussed: periodic, quasi-periodic, chaotic and hyperchaotic. Results show that the 0–1 test is capable to distinguish regular and irregular signals being compatible with other tools. In brief, p–q dynamics exhibits bounded behavior represented by closed curves associated with regular solutions (periodic and quasi-periodic); and irregular unbounded behavior related to irregular dynamics (chaos or hyperchaos). Only the estimation of Lyapunov spectrum is capable to distinguish periodic and quasi-periodic behaviors or chaos and hyperchaos. In this sense, the 0–1 test is similar to the maximum Lyapunov exponents. Nevertheless, it is easier to be applied and it is necessary neither to define algorithm parameters nor to perform state space reconstruction. Concerning the different K-Metrics that can be implemented in the 0–1 test, the various possibilities give equivalent results in terms of the final indicator of chaoticity. As a matter of fact, even if different dependences on the parameter c may arise with the different metrics, the final indicators given by the median values over all values of parameter c, agree to give the same diagnostic result irrespective of the chosen metric. Notwithstanding, the correlation metrics are less c-dependent. On the basis of the numerical simulations carried out with different constitutive models, different dynamical systems as well as different types of trajectories, the authors believe that 0–1 test is an interesting, reliable and computationally efficient tool to diagnose chaotic behavior in SMA systems where the calculation of Lyapunov exponents are difficult to be employed.

Acknowledgments

The authors would like to acknowledge the support of the Brazilian Research Agencies CNPq (302.709/2013-4), CAPES and FAPERJ (E-26/202.985/2015). The Air Force Office of Scientific Research (AFOSR (FA9550-16-0381)) is also acknowledged. GL is grateful for the Foundation for Polish Science support.

References

[1] Aguiar RAA, Savi MA, Pacheco PMCL. Experimental investigation of vibration reduction using shape memory alloys. J Intell Mater Syst Struct 2013;24(2):247–61.
[2] Bernardini D, Litak G. An overview of 0-1 test for chaos. J Brazilian Soc Mech Sci Eng 2016;38:1433–50.
[3] Bernardini D, Pence TJ. Uniaxial modeling of multivariant shape-memory materials with internal sublooping using dissipation functions. Meccanica 2005;40:339–64.
[4] Bernardini D, Rega G. Thermomechanical modeling, nonlinear dynamics and chaos in shape memory oscillators. Math Comput Model Dyn Syst 2005;11:291–314.
[5] Bernardini D, Rega G. Chaos robustness and strength in thermomechanical shape memory oscillators. Part I: a predictive theoretical framework for the pseudoelastic behavior. Int J Bifurcation Chaos 2011;21(10):2769–82.
[6] Bernardini D, Rega G. Chaos robustness and strength in thermomechanical shape memory oscillators. Part II: numerical and theoretical evaluation. Int J Bifurcation Chaos 2011;21(10):2783–800.
[7] Bernardini D, Rega G, Litak G, Syta A. Identification of regular and chaotic isothermal trajectories of a shape memory oscillator using the 0-1 test. Proc. Inst. Mech. Engineers Part K-J. Multi-Body Dyn. 2012;227(1):17–22.
[8] Enemark S, Savi MA, Santos IF. Nonlinear dynamics of a pseudoelastic shape memory alloy system: theory and experiment. Smart Mater Struct 2014;23(8) Article 085018.
[9] Enemark S, Savi MA, Santos IF. Experimental analyses of dynamical systems involving shape memory alloys. Smart Struct Syst 2015;15(6):1521–42.
[10] Falconer I, Gottwald GA, Melbourne I, Wormnes K. Application of the 0-1 test for chaos to experimental data. SIAM J Appl Dyn Syst 2007;6(2):395–402.
[11] Falk F. Model free-energy, mechanics and thermodynamics of shape memory alloys. Acta Metall 1980;28:1773–80.
[12] Feng ZC, Li DZ. Dynamics of a mechanical system with a shape memory alloy bar. J Intell Mater Syst Struct 1996;7:399–410.
[13] Fraser AM, Swinney HL. Independent coordinates for strange attractors from mutual information. Phys Rev A 1986;33:1134–40.
[14] Gottwald GA, Melbourne I. A new test for chaos in deterministic systems. In: Proceedings of the royal society london A, 460; 2004. p. 603–11.
[15] Gottwald GA, Melbourne I. Testing for chaos in deterministic systems with noise. Physica D 2005;212:100–10.
[16] Gottwald GA, Melbourne I. On the implementation of the 0-1 test for chaos. SIAM J Appl Dyn Syst 2009;8:129–45.
[17] Gottwald GA, Melbourne I. On the validity of the 0-1 test for chaos. Nonlinearity 2009;22:1367–82.
[18] Gottwald GA, Melbourne I. The 0-1 test for chaos: a review. In: Chaos detection and predictability, 915; 2016. p. 221–47. of the series Lecture Notes in Physics.
[19] Hegger R, Kantz H, Schreiber T. Practical implementation of nonlinear time series methods: The TISEAN package. Chaos 1999;9(2):413–35.
[20] Kantz H. A robust method to estimate the maximal Lyapunov exponent of a time series. Phys Lett A 1994;185:77–87.

[21] Krese B, Govekar E. Nonlinear analysis of laser droplet generation by means of 0–1 test for chaos. Nonlinear Dyn 2012;67:2101–9.
[22] Lagoudas, DC. (2008), "Shape memory alloys: modeling and engineering applications", Springer Science Business Media.
[23] Litak G, Syta A, Wiercigroch M. Identification of chaos in a cutting process by the 0-1 test. Chaos Solit Fract 2009;40:2095–101.
[24] Machado LG, Savi MA, Pacheco PMCL. Nonlinear dynamics and chaos in coupled shape memory oscillators. Int J Solids Struct 2003;40(19):5139–56.
[25] Machado LG. Shape memory alloys for vibration isolation and damping PhD Thesis. Texas A&M University, Department of Aerospace Engineering; 2007.
[26] Machado LG, Lagoudas DC, Savi MA. Lyapunov exponents estimation for hysteretic systems. Int J Solids Struct 2009;46(6):1269–86.
[27] Paiva A, Savi MA, Braga AMB, Pacheco PMCL. A constitutive model for shape memory alloys considering tensile-compressive asymmetry and plasticity. Int J Solids Struct 2005;42(11–12):3439–57.
[28] Rhodes C, Morari M. False-nearest-neighbors algorithm and noise-corrupted time Series. Phys Rev E 1997;55(5):6162–70.
[29] Savi MA. Nonlinear dynamics and chaos of shape memory alloy systems. Int J Non Linear Mech 2015;70:2–19.
[30] Savi MA, Sá MAN, Paiva A, Pacheco PMCL. Tensile-compressive asymmetry influence on shape memory alloy system dynamics. Chaos Solit Fract 2008;36:828–42.
[31] Savi MA, Pacheco PMLC. Chaos and hyperchaos in shape memory systems. Int J Bifurcation Chaos 2002;12(3):645–57.
[32] Savi MA, Braga AM. Chaotic vibration of an oscillator with shape memory. J Brazilian Soc Mech Sci 1993;15(1):1–20.
[33] Sitnikova E, Pavlovskaia E, Ing J, Wiercigroch M. Suppressing nonlinear resonances in an impact oscillator using SMAs. Smart Mater Struct 2012;21(7) Article 075028.
[34] Takens F. Detecting strange attractors in turbulence. In: Rand D, Young L-S, editors. Lecture notes in mathematics, 898. Springer; 1981. p. 366–81.
[35] Webel K. Chaos in German stock returns - new evidence from the 0-1 test. Econ Lett 2012;115(3):487–9.
[36] Wolf A, Swift JB, Swinney HL, Vastano JA. Determining Lyapunov exponents from a time series. Physica 1985;16D:285–317.
[37] Yang Y, Ren X, Qin W. Two novel methods for vibration diagnosis to characterize non-linear response. Nonlinear Anal 2008;68:582–90.
[38] Yuan L, Yang Q, Zeng C. Chaos detection and parameter identification in fractional-order chaotic systems with delay. Nonlinear Dyn 2013;73:439–48.